Euro. Jnl of Applied Mathematics (2004), *vol.* 15, *pp.* 853–871. © 2004 Cambridge University Press
doi:10.1017/S0956792504005674 Printed in the United Kingdom

Air-water interactions near droplet impact

R. PURVIS and F. T. SMITH

Mathematics Department, Univeraity College London, Gower Street, London WC1E 6BT, UK
email: frank@math.ucl.ac.uk

(*Received 24 November 2003; revised 28 May 2004*)

The effects of the thin air layer entering play when a water droplet impacts on otherwise still water or on a fixed solid are studied theoretically with special attention on surface tension and on post-impact behaviour. The investigation is based on the small density and viscosity ratios of the two fluids. In certain circumstances, and in particular for droplet Reynolds numbers below a critical value which is about ten million, the air-water interaction depends to leading order on lubricating forces in the air coupled with potential flow dynamics in the water. The nonlinear integro-differential system for the evolution of the interface and induced pressure is studied for pre-impact surface tension effects, which significantly delay impact, and for post-impact interaction phenomena which include significant decrease of the droplet spread rate. Above-critical Reynolds numbers are also considered.

1 Introduction

The present theoretical work is motivated mainly by the air-water interactions induced when a water droplet impinges on a body of water, a particular industrial context being in terms of the icing-up of a wing beneath that body of water. Examples of air-water interactions are observed in the experiments shown by Lesser & Field (1983), Liow (2001) and in direct numerical simulations by Gueyffier *et al.* (1999), Josserand & Zaleski (2003) and Purvis & Smith (2004). A recent review given in Smith *et al.* (2003) discusses relevant literature, including interesting papers by Howison *et al.* (1991, 2002), Wilson (1991) and Korobkin (1997, 1999) on inviscid aspects, and by King & Tuck (1993), King, Tuck & Vanden-Broeck (1993), Vanden-Broeck & Miloh (1996) and Vanden-Broeck (2001) on viscous/inviscid waves of steady or travelling type. The Smith *et al.* analysis is, however, perhaps the most relevant one here as it found a critical droplet Reynolds number below which the air has a lubricating action and above which the air acts as if inviscid. Moreover, that critical Reynolds number is of the order of 10 million, thus pointing (rather surprisingly) to the use of lubrication theory in the many practical contexts such as that mentioned at the beginning where the typical value of Reynolds number is less than about 100,000. The predictions from the analysis are also in qualitative agreement with the Lesser & Field experimental results among others.

In the real situations of present background concern the droplet Reynolds number (Re_1, where the subscript 1 signifies the value for water) and Weber number (We_1) are both large, in fact, typically around 10,000–100,000, and the Froude number tends to be greater still. These values are based on the characteristic water droplet diameter, approach

velocity, density, kinematic viscosity and air-water surface tension. Gravity can usually be neglected at least over the shorter term of an impact but surface tension effects (cf. Kriegsmann *et al.* (1998), McKinley & Wilson (2001), Miksis & Vanden-Broeck (1999) and Kang & Vanden-Broeck (2000)) would seem to require detailed examination despite the largeness of the representative Weber number.

There are many interaction effects present in the real/industrial setting of course. The current concern is with two main aspects, namely surface tension and post-impact phenomena. The droplet of water may be taken to fall vertically on to an otherwise still horizontal thick layer of water, for definiteness. The interaction with the air motion induced in the relatively thin gap between the two bodies of water is then the concern here just prior to or soon after impact takes place, and, as in most related works, a planar incompressible regime is assumed. Similar reasoning applies to impact onto a fixed solid wall and also more generally to any two fluids, say fluids 1 and 2, with small density and viscosity ratios. These ratios are in fact treated as vanishingly small parameters (Smith *et al.*) in the present investigation.

The comparatively small-time response can be addressed analytically to account for air cushioning or for pre-existing air flow, both of which are of practical relevance, although this work concentrates only on the former for the most part. The overall aim is to understand more of the complex short term dynamics near impact and also longer term features such as the nature of any fluid splash, although again the current work is concerned only with the former. An alternative or complement is direct numerical simulation (e.g. Gueyffier *et al.*, 1999; Josserand & Zaleski, 2003; Purvis & Smith, 2004, 2005), which provides helpful comparisons as well as capturing the broader longer term behaviour in principle.

§2 describes the structure of the air-water interaction for pre-impact surface tension effects and also for post-impact behaviour; we should emphasize that these are treated throughout as separate issues. The Reynolds number is taken to lie below the critical value, in the main text. Solution properties are considered in §3 for the pre-impact case and in §4 post-impact including for example the influence of a wall roughness. Our interest is mostly in the water-air-water configuration but the reasoning holds virtually unchanged for water-air-solid, as noted already. In the latter configuration it is worth pointing out that the dynamics near the contact point of §4 is found to be predominantly inviscid. A final discussion is provided in §5, while an appendix considers the behaviour at above-critical Reynolds numbers.

2 Air-water interaction

Nondimensional variables are used in which the velocity $\underline{u} = (u, v)$, the corresponding Cartesian coordinates (x, y), the pressure p and the time t are based on the droplet approach speed V, a representative length scale D, $\rho_1 V^2$ and D/V, respectively. Here D is a global quantity such as the droplet diameter if the droplet is of circular shape, while ρ_1 is the density of the water (or fluid 1). The Navier–Stokes equations then take the form, in the water,

$$(\partial_t + \underline{u} \cdot \nabla)\,\underline{u} = -\nabla p + \mathrm{Re}_1^{-1} \nabla^2 \underline{u}, \tag{2.1a}$$

with ∇ denoting the operator (∂_x, ∂_y), and in the air (fluid 2)

$$(\partial_t + \underline{u}\cdot\nabla)\,\underline{u} = -\left(\frac{\rho_1}{\rho_2}\right)\nabla p + \left(\frac{\nu_2}{\nu_1}\right)\mathrm{Re}_1^{-1}\nabla^2\underline{u}. \tag{2.1b}$$

Here $\mathrm{Re}_1 \equiv VD/\nu_1$ is the droplet Reynolds number, $\mu_1 = \rho_1\nu_1$ denoting the viscosity of the water. Gravity is neglected here: see later. The air density and viscosity are $\rho_2, \mu_2 (= \rho_2\nu_2)$, respectively. The continuity equation

$$\nabla\cdot\underline{u} = 0 \tag{2.1c}$$

applies in each fluid. The coordinates used are centred for convenience in the impact area. The pressure is measured relative to the atmospheric value.

The impact setting has rapid local interaction involving a thin layer of air between water and a solid surface or between two bodies of water, depending on whether the droplet impacts on a solid or on water. The theory takes the density and viscosity ratios of the two fluids 1,2, that is ρ_2/ρ_1 and μ_2/μ_1, to be small; for dry air with pure water these two ratios are near $1/828$ and $1/55$ in turn, at 20° C and one-atmosphere pressure, while at 0.1° C the ratios are near $1/772$ and $1/100$. With that background, and with the aspect ratio δ of the air layer assumed small, asymptotic expansions for the velocities and pressure in the two fluids are substituted into (2.1a–c) in principle regardless of whether the behaviour is pre- or post-impact. The expansions follow from an order of magnitude argument. Thus

$$(u, v, p) = \begin{cases} (u_1, v_1, \delta^{-1}p_1) + \cdots & \text{in the water,} \\ (\delta^{-1}u_2, v_2, \delta^{-1}p_2) + \cdots & \text{in the air,} \end{cases} \tag{2.2a,b}$$

with the typical time scale $t = \delta^2 T$ being short ($T \sim 1$). The length scalings in the water are also short near impact, $(x, y) = (X, Y)a/D$ where the characteristic local length $a \ll D$ (indeed $a/D \sim \delta$ for a smooth incident droplet shape), while in the air layer which lies astride the x-axis the scalings are $(x, y) = (X, \delta\hat{y})a/D$. The governing equations in the water are therefore those of unsteady potential flow, while those in the air are of lubrication. Hence interaction is controlled by the coupled equations

$$F_{TT} = \frac{1}{\pi}\int_{-\infty}^{\infty} P_\xi(\xi, T)\frac{d\xi}{X-\xi}, \tag{2.3}$$

$$(F^3 P_X)_X = (12\Gamma)F_T, \tag{2.4}$$

for the unknown scaled interface shape $F(X, T)$ and pressure $P(X, T)$. Here $p_2(X, \hat{y}, T) = p_1(X, 0, T) \equiv P$ to leading order and (2.3) follows from the water flow equations subject to the kinematic condition at the interface and to uniform approach motion in the farfield, whereas (2.4) is Reynolds lubrication equation from the air motion. The pressure P must tend to zero at large $|X|$ in view of the atmospheric pressure. So far this is for the case of droplet impact on a solid. For impact onto water, in which case (2.1a), (2.2a) apply in each body of water, the factor 12Γ is replaced by 3Γ as F represents essentially the average $(F_1 + F_2)/2$ of the dual water-air and air-water interfacial shapes, with P as their common pressure.

The parameter Γ denotes $\mu_2/(\delta^3\rho_1 VD)$ and is taken as 0(1). The validity of (2.3), (2.4) relies on several assumptions which are met readily in real applications, namely that δ is large relative to ρ_2/ρ_1 but small relative to both ρ_1/ρ_2 and $(\mu_2/\mu_1)^{1/3}$, and the global Reynolds number Re_1 is comparable with $\mu_2/(\mu_1\delta^3)$. Hence the theory applies for Re_1 values that are large but lie below about $v_2\rho_1^2/(v_1\rho_2^2)$, a critical value which is more than 10^7 for the air-water combination.

Solutions of (2.3), (2.4) are described in Smith *et al.* (2003) for pre-impact behaviour, usually with the normalized condition

$$F \sim X^2 - T, \quad \text{for } T \to -\infty \text{ or } |X| \to \infty, \tag{2.5}$$

which is appropriate to the incident locally parabolic shape of the interface when or where interaction is still weak, and in line with $v \to -1$ in the incident motion. The solutions show that as the interaction strengthens it leads to a so-called touchdown, meaning that $F \to 0$ at one or more positions X within a finite time T.

The extra effects of gravity and compressibility are also considered in that paper, but here our concern is with the influence of surface tension in the pre-impact stage (§ 3) and, separately, with the application to post-impact phenomena (§ 4). The inclusion of surface tension leads to (2.3) being replaced by

$$F_{TT} = \frac{1}{\pi} \int\!\!\!\!\!\!- _{-\infty}^{\infty} [P_\xi(\xi, T) + \sigma F_{\xi\xi\xi}(\xi, T)] \frac{d\xi}{X - \xi}, \tag{2.6}$$

where the parameter σ is regarded here as $O(1)$. The reason for this is the difference between the water pressure and the air pressure ($\propto P$) being the surface tension multiplied by the interfacial curvature, which is proportional to $\partial^2 F/\partial X^2$ in the present context. The scaled air pressure P must still tend to zero at large $|X|$ whereas the water pressure tends to 2σ, given (2.5).The parameter σ is the dimensional surface tension multiplied by $\delta^2/(\rho_1 V^2 a)$ and so is of order δ/We_1 which in practice is numerically quite small for our current applications described in the introduction. Again, the implications of (2.3), (2.4) for post-impact behaviour can be investigated given that the argument leading to them holds equally well after an impact as long as we allow for the air gap being closed in at least one interval of the domain. Thus

$$F = 0 \text{ for } X_1 < X < X_2 \tag{2.7}$$

say, where the unknown positions X_1, X_2 vary with T in general. The repercussions from (2.6), (2.7) respectively are considered in the following two sections.

3 Pre-impact behaviour: surface tension effects

Addressing (2.4) with (2.6), we sought numerical solutions by modifying the method in Smith *et al.* (2003). In brief, this uses fourth order accurate compact differencing in X accompanied by global iteration at each time level, together with a second order temporal treatment, starting from initial conditions imposed at a suitably large negative time. After some trials, suitable representative grids in X were found to have steps of 0.05 between

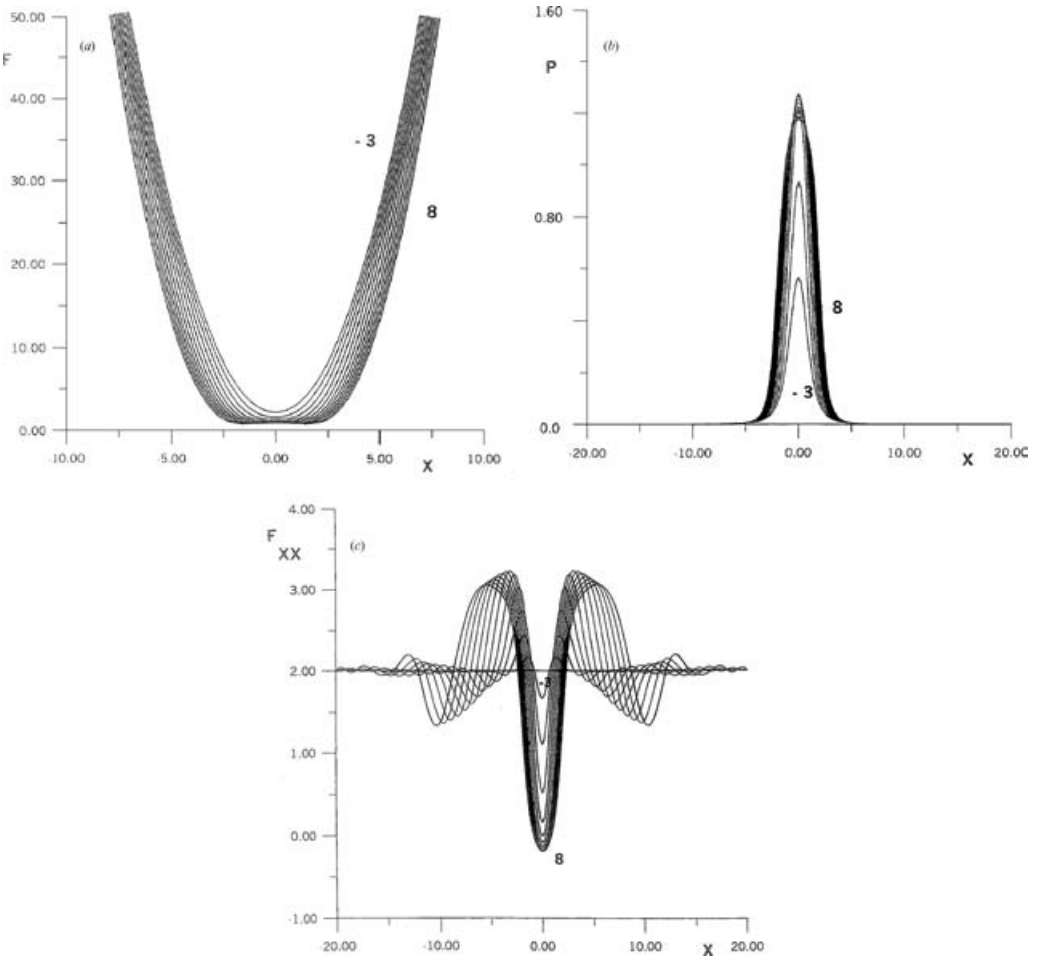

FIGURE 1. (a–c) F, P, F_{XX} versus X at times $T = -3$ to 8, as shown.

endpoints at ± 20, whereas 0.001 is the typical time step, although the suitability depends also on the value of the surface tension parameter.

Results for a specific nonzero σ value, namely 0.4, are presented in Figure 1(a–c). Here plots of F, P and the effective curvature $\partial^2 F/\partial X^2$ in turn against X are given at various times T. In Figure 1(a) small waves are present in the F profiles in an outer portion of the solution but they are discernible only on very close scrutiny, whereas the waves are far more apparent in Figure 1(c). (In response to a referee's remark, these waves and their propagation may indeed be viewed as causing the delay in impact discussed later.) Figure 1(b), which is shown on a scale similar to Figure 1(c) to compare them readily, points to some decay of P in a middle portion at increased T with P then falling towards 2σ. We note that P tends to zero as $|X| \to \infty$ strictly (in line with P being the scaled pressure in the air gap), and indeed a relatively steep and monotonic rise or fall to that asymptote is indicated in Figure 1(b) as $|X|$ increases. Figure 1(c)'s middle portion is characterised by $\partial^2 F/\partial X^2$ becoming very close to $2 - P/\sigma$ (see analysis below), and hence

exhibiting a relatively steep rise with increasing $|X|$, near the edge of that middle portion, while being relatively near zero within that portion. Outside, however, waves as an extra feature are clearly seen; eventually as T increases they persist to the outer boundary, which is here at ± 20, and this can lead to unrealistic growth in the numerical solution. Further, in comparison with the zero-σ case of Smith *et al.* (2003), the major effects of adding surface tension are initially small, over this parameter range, but they are very telling in the long run for the following reason. The main indication from the results is that the solution for any positive σ continues for all time T, unlike that for zero σ which touches down in a finite T: see also the final paragraph of this section.

With σ positive the interface shape F continues to drop slowly within a middle portion of the X axis, then, at increased times, but rises fast in spatial terms quite locally and waves are induced in a region outside of that. Indeed, the solution for $\sigma > 0$ appears to acquire the following form at large positive times. Suppose the solution F rises relatively fast in spatial terms, in a local zone near $X = cT^n$ say, with the constant c positive, such that the length scaling has

$$X = cT^n + T^m \bar{X} \text{ (as } T \to \infty). \tag{3.1}$$

For the zone to be local the unknown powers m, n must satisfy $m < n$, with $\bar{X}$ of $O(1)$ here, while corresponding expansions of the interface shape F and pressure P are assumed in a fairly general form

$$F = T^{\lambda} \bar{F}(\bar{X}) + \cdots, \tag{3.2a}$$

$$P = T^{\lambda - 2m} \bar{P}(\bar{X}) + \cdots, \tag{3.2b}$$

as indicated by the integrand in (2.6) and by the computational results. The power λ is also unknown. The system (2.4), (2.6) then reduces to

$$\sigma(\bar{F}^3 \bar{F}''')' = (12\Gamma) c \bar{F}', \tag{3.3}$$

with a prime here denoting $d/d\bar{X}$, subject to

$$m = \lambda + (1 - n)/3, \qquad 3\lambda < 5(1 - n), \tag{3.4a,b}$$

and also $3\lambda < (4n - 1)$. The balance (3.4a) stems from (2.4) and (3.4b) from (2.6) assuming that the double temporal derivative is negligible. Integration of (3.3) yields

$$\frac{\sigma}{(12\Gamma)} \bar{F}^3 \bar{F}''' = c\bar{F} - c_1 \tag{3.5}$$

where c_1 is a constant of integration. See also Greenspan (1978), Tuck & Schwartz (1990), Kalliadasis & Chang (1994), Beretta (1997), Jensen (2000) and Braun & Fitt (2003) concerning properties of (3.5). The local solution $\bar{F}$ is expected to tend to a nonzero constant, c_1/c, as $\bar{X}$ tends to $-\infty$. So $c_1 > 0$. An exact solution is $\bar{F} \equiv c_1/c$ for all $\bar{X}$, which is associated with the form in the middle portion on the left remaining unaltered (the middle portion has F being almost constant spatially). However, perturbations from this can occur, with

$$\bar{F} \sim c_1/c + \gamma_1 \exp(\gamma_2 \bar{X}) \text{ as } \bar{X} \to -\infty, \tag{3.6a}$$

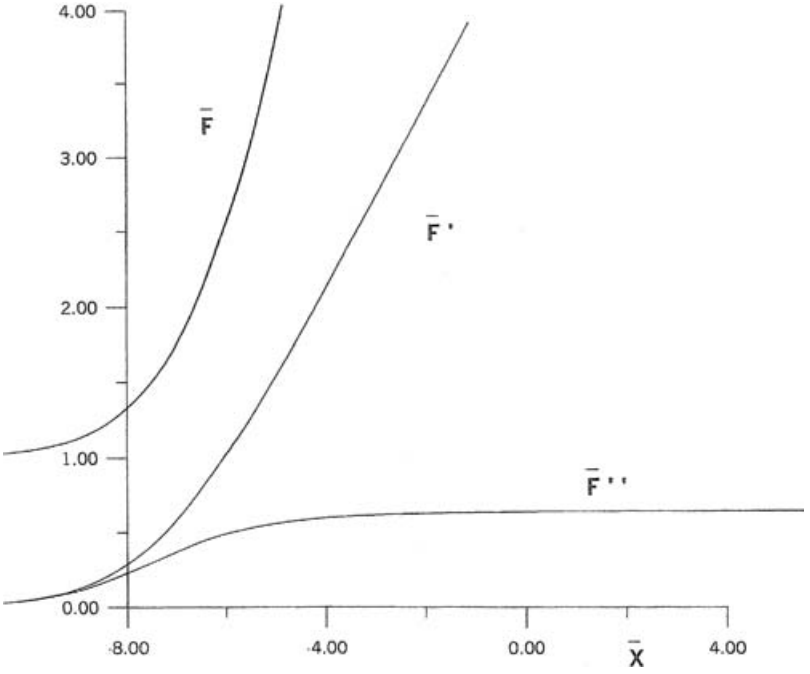

FIGURE 2. $\bar{F}, \bar{F}', \bar{F}''$ against $\bar{X}$, from (3.5) subject to (3.6a,b) with $\gamma_1 > 0$ and $\sigma/(12\Gamma), c, c_1$ normalized to unity.

and the positive root γ_2 follows from (3.5) as

$$\gamma_2 = c_1^{-1} c^{4/3} (12\Gamma/\sigma)^{1/3}, \tag{3.6b}$$

whereas γ_1 remains arbitrary. Computed results for the nonlinear solution of (3.5) with the starting form (3.6a,b) were derived from a forward marching finite difference method and are presented in Figure 2. In the figure $\bar{F}, \bar{F}', \bar{F}''$ are plotted against $\bar{X}$, with the constants $\sigma/(12\Gamma)$, c, c_1 all having been normalized to unity without loss of generality via a division of $\bar{F}$, $\bar{X}$ by c_1/c, $(\sigma c_1^3/(12\Gamma c^4))^{1/3}$ in turn. The results shown are for $\gamma_1 > 0$, and in fact any positive value of γ_1 leads to the same solution modulo an origin shift in $\bar{X}$. (A negative γ_1 value produces in contrast quite different features, dominated by a singular response in $\bar{F}$ at a finite $\bar{X}$ value). The behaviour obtained at large positive $\bar{X}$ is in keeping with the asymptote

$$\bar{F} \sim \gamma_3 \bar{X}^2 \text{ as } \bar{X} \to \infty \tag{3.7}$$

where γ_3 is a positive constant. It is interesting that the asymptotes (3.6a), (3.7) give

$$\bar{P}(\infty) - \bar{P}(-\infty) = -2\sigma\gamma_3, \tag{3.8}$$

suggesting a negative quasi-jump in pressure across the present zone, cf. Figure 1(b)'s results.

In view of (3.7) with (3.1), (3.2a), F emerges as

$$F \sim \gamma_3 T^{2(n-1)/3-\lambda}(X - cT^n)^2 \tag{3.9}$$

just to the right of the local zone. The farfield condition (2.5) then indicates that the powers are related by

$$n = 1 + 3\lambda/2, \quad m = \lambda/2, \tag{3.10}$$

as far as the X^2 requirement is concerned. In (3.10) λ can lie between -1 and zero. Further, waves are induced in the portion to the right of the above local zone essentially because of the $-T$ requirement in (2.5) compared with the property (3.9) at $X = cT^n+$. The waves are inviscid capillary waves due to the balance

$$F_{TT} \sim \frac{\sigma}{\pi} \int\!\!\!\!\!\!- _{-\infty}^{\infty} F_{\xi\xi\xi}(\xi, T) \frac{d\xi}{X - \xi} \tag{3.11a}$$

as the double temporal derivative comes into play on the right. The balance (3.11a) yields

$$F \sim X^2 - T + \frac{1}{2\pi} \int_{-\infty}^{\infty} H(\omega) \exp\left\{ i\big(\omega X - \sigma^{1/2}|\omega|^{3/2} T\big) \right\} d\omega \tag{3.11b}$$

where the Fourier transform function $H(\omega)$ is effectively from an initial distribution. The major contribution to (3.11b) at large T comes from $\omega = 4\eta^2/(9\sigma) + t^{-1/2}\eta^{-1/2}\tilde{\omega}$, with $\tilde{\omega}$ of 0(1) and $\eta \equiv X/T$, and is proportional to

$$T^{-1/2}\eta^{1/2} H(4\eta^2/(9\sigma)) \cos\left(\frac{4\eta^3 T}{27\sigma} - \frac{\pi}{4} \right), \tag{3.11c}$$

which shows a main X-scale expanding like T but including a relatively fast wave of scale $|X| \sim T^{2/3}$ and of decaying amplitude. Again, this seems in line with the computed trends in Figure 1.

If λ is zero then $n = 1,\ m = 0$ and so the double temporal derivative in (2.6) reasserts itself, bringing in the principal-value integral and pointing to a nonlinear travelling wave form. Now $X - cT \equiv \bar{X}$ and, in the local zone, F, P depend only on $\bar{X}$ to leading order and satisfy

$$c^2 F'' = \frac{1}{\pi} \int\!\!\!\!\!\!- _{-\infty}^{\infty} [P' + \sigma F'''] \frac{d\xi}{\bar{X} - \xi}, \tag{3.12a}$$

$$(F^3 P')' = -(12\Gamma) c F', \tag{3.12b}$$

from (2.4), (2.6). Each of (3.12a,b) can be integrated fairly readily once in $\bar{X}$. For large σ and/or small c however the previous nonlinear form (3.3), (3.5)–(3.8) is reinstated where the $|\bar{X}|$ scale is not excessive and the linear form (3.11a–c) on the right then follows where $|\bar{X}| \sim \sigma c^{-2}$. For zero σ, moreover, (3.12a,b) has already been studied in Smith *et al.* (2003, section 5). In addition, it should be mentioned that we have performed time-marching calculations on the reduced system where (2.6) is dominated by the $\partial P/\partial X$ and $\partial^3 F/\partial X^3$ contributions (cf. Greenspan (1978), Beretta (1997), Braun & Fitt (2003)), for example with large surface tension parameter and limited $|X|$ scale. This, coupled with (2.4) and the condition (2.5), leads to broad trends similar to those of the full system, including the asymptote (3.1)–(3.10) and a right-hand region of adjustment. The account (3.1)–(3.12)

overall appears to capture the essence of the large-time features, confirming the absence of a touchdown in the present regime of (2.4), (2.6).

Finally here, it is interesting to examine how small-σ effects come into reckoning given that the zero-σ case touches down ($F \to 0$) at a finite time $T = T_t$ say. The contribution $\sigma\partial^2 F/\partial X^2$ due to surface tension is large and of order $\sigma(T_t - T)^{-2}$ in the touchdown structure of Smith *et al.* (2003) compared with the scaled pressure P, which is also large but has the order $(T_t - T)^{-1/2}$. Hence the surface-tension contribution asserts its influence only when $(T_t - T)$ becomes as small as $\sigma^{2/3}$, i.e. in a time scale of order $\sigma^{2/3}\delta^2$ in t. That scale within the present model seems to account entirely for the boundary between touchdown (impact) and inhibited impact as it tends to reinstate a fuller system close to (2.4), (2.6) but with σ replaced by unity, allowing the terminal form of (3.1)–(3.12) to be approached then. In practical terms, this time scale and the corresponding spatial scales are tiny.

4 Post-impact interactions

The arguments and main equations of §2 also apply after an impact but subject to the condition (2.7), which corresponds to the existence of a finite interval of contact. Here, to repeat, the surface tension effect is neglected, and in addition we consider a symmetric impact in which $X_1 = -X_2$ with $X_2 = \ell(T) > 0$ being the unknown half-length of contact, while the unknown interface shape F is even in X. Building the requirements of (2.7) as well as symmetry into the system (2.3), (2.4) and for convenience setting $\partial F/\partial T$ as Q leads to a problem involving Wiener-Hopf techniques to deal with the mixed boundary conditions which are (2.7) within the contact interval but (2.4) outside. This, with allowance for the square-root shape of F near the contact point, then points to the governing equations

$$Q_T - \frac{\tilde{X}\ell'}{\ell}Q_{\tilde{X}} = -\frac{\hat{v}\tilde{X}}{(\tilde{X}^2-1)^{3/2}\ell^2} + \frac{2\tilde{X}}{\pi\ell(\tilde{X}^2-1)^{1/2}}\int_1^\infty \frac{(\xi^2-1)^{1/2}P_\xi\, d\xi}{(\tilde{X}^2-\xi^2)}, \tag{4.1a}$$

$$F_T - \frac{\tilde{X}\ell'}{\ell}F_{\tilde{X}} = Q, \tag{4.1b}$$

$$(F^3 P_{\tilde{X}})_{\tilde{X}} = (12\Gamma)\ell^2 Q, \tag{4.1c}$$

for F, Q, P as functions of $\tilde{X}, T$. The coordinate $\tilde{X} \equiv X/\ell(T)$ has also been introduced here in order to fix the contact point at $\tilde{X} = 1$. Hence our concern is with the domain $\tilde{X} > 1$ due to the assumed symmetry, without which the different solutions in two domains would need to be considered. Also $\hat{v}(T)$, like $\ell(T)$, is to be found; $\hat{v}(T)$ is the coefficient of the eigenfunction (the first term on the right of (4.1a)) associated with the Wiener-Hopf inversion and it is related to the variation in the length of the contact domain $|X| < \ell(T)$ via (4.2e) below. The condition (2.5) still holds in the far field.

Mention should be made here of two other parts of the flowfield. One is a linear viscous-inviscid 'jet-root' region closer to the moving contact point at $X = \ell, \tilde{X} = 1$, implied by the local square-root behaviour of the shape F (see (4.2a) below). The region has extent $0(\delta/\mathrm{Re}_1)$ in both y and $x - \delta\ell(T)$ and so is small with respect to the main scales given earlier. Its velocities and pressure have the respective orders $\mathrm{Re}_1^{1/2}, \delta^{-1}\mathrm{Re}_1^{1/2}$,

implying that the linearized steady Navier-Stokes equations hold in scaled terms in the coordinate frame moving with the contact point; this is for the local water motion alone since the air effect is negligible near the contact point. In consequence, the local length scales are larger than, and the local problem is distinct from, the purely inviscid case of Howison *et al.* (1991). The solution here, which must satisfy zero-pressure conditions at the unknown interface among other conditions, is unknown. For the case of impact onto a solid surface, the solution is felt likely to show that a jet must emerge horizontally from the region, with typical velocity of order $\mathrm{Re}_1^{1/2}$ at most and width of order δ/Re_1 initially. That leads, second, into a thin water 'jet' layer just beneath the air gap, over the horizontal length scale where $x \sim \delta$ and air effects are important. The horizontal water layer then has a characteristic horizontal velocity which, although large, is initially small relative to the air velocities, from (2.2b); hence, more accurately, the 'jet' is a comparatively thin water layer bounded above by an interface with the air. Also, the typical water-layer mass flux is only $O(\delta \mathrm{Re}_1^{-1/2})$, relatively small compared with that of $0(\delta)$ in the air flow. This flux is consistent with the kinematic condition on v at the interface. Likewise the water-layer momentum is comparatively small, by a relative factor $O(\delta)$, compared with that in the air flow. The influence on the main water-air dynamics appears to be negligible from both of these other regions. The same conclusion applies for water-air-water impact, where the thin water layer slices through the air gap; the pressure jump induced across the water layer due to its momentum is small compared with the air pressures which are large and $O(\delta^{-1})$, from (2.2b), over the $O(\delta)$ length scale. We therefore return to the main post-impact interaction between water and air on the $x \sim \delta$ length scale, i.e. to (4.1a–c).

With the constant Γ zero, so that the air dynamics is neglected, the solution of (4.1a–c) has P identically zero and $\ell \sim (2T)^{1/2}$, $\hat{v} \to 1$ (Korobkin, 1997, 1999; Howison *et al.*, 2002). That applies at any finite T if the starting conditions are ideal but otherwise asymptotically for T large and positive.

With the constant Γ nonzero, the system (4.1a–c) needs a numerical treatment in general. This was adapted from that in the previous section principally to allow for the square-root factors in (4.1a) and for the inherent irregular behaviour near contact, by means of a transformation $\tilde{X} = 1 + \tan^2(\chi)$. The behaviour as $\tilde{X} \to 1+$ is perhaps best encapsulated by expanding F around any particular time instant T_* as $F_0 + (T - T_*)F_1 + \cdots$ and similarly for the other variables around that instant and then writing, for integers $n \geqslant 0$,

$$F_n \sim a_n(\tilde{X} - 1)^{1/2} + b_n(\tilde{X} - 1)^{3/2} + \cdots, \tag{4.2a}$$

$$Q_n \sim \alpha_n(\tilde{X} - 1)^{-1/2} + \beta_n(\tilde{X} - 1)^{1/2} + \cdots, \tag{4.2b}$$

$$dP_n/d\tilde{X} \sim \pi_n(\tilde{X} - 1)^{-1} + \cdots. \tag{4.2c}$$

Then from (4.1a–c) the first few constants satisfy

$$-\frac{\ell_1 a_0}{2\ell_0} = \alpha_0, \quad a_1 - \frac{\ell_1}{\ell_0}\left(\frac{a_0}{2} + \frac{3b_0}{2}\right) = \beta_0, \tag{4.2d}$$

$$\frac{\ell_1 \alpha_0}{\ell_0} = \frac{-\hat{v}_0}{2^{1/2}\ell_0^2}, \quad a_0^3 \pi_0 = 24\Gamma \ell_0^2 \alpha_0, \quad \alpha_1 + \frac{\ell_1}{2\ell_0}(\alpha_0 - \beta_0) = -\frac{\hat{v}_0}{2^{7/2}\ell_0^2} + \phi_0. \tag{4.2e}$$

These determine $\ell_1, a_1, \hat{v}_0, \pi_0, \alpha_1$ in turn for given $a_0, b_0, \alpha_0, \beta_0$ and ℓ_0, etc., and confirm that

the dominant response near contact is in effect air-free and hence inviscid. Again, from the first equation in (4.2e) $\hat{v}$ plays a role in determining the local growth of the contact domain. In the third equation of (4.2e) the constant ϕ_0 is given by

$$\phi_0 = -\frac{2^{1/2}}{\ell_0 \pi} \int_1^\infty \left[\frac{dP_0}{d\xi} - \frac{2^{1/2}\pi_0}{(\xi - 1)(\xi + 1)^{1/2}} \right] \frac{d\xi}{(\xi^2 - 1)^{1/2}} + \frac{\pi_0}{2^{1/2}\ell_0}, \tag{4.3}$$

in which the integral is finite in view of (4.2c) and the relative corrections which are $O(\tilde{X} - 1)$ throughout; the integral represents a global influence from the air motion on the near-contact properties. The main relations among (4.2a–e) were incorporated as local requirements into the overall computational scheme. To step forward by a small time step, from old to new time, the program used assumes that F, Q, P (at stations for all $\tilde{X} > 1$) and $\ell, \hat{v}$ are known at the old time. Then new $\ell, \hat{v}$ values are inferred from the local behaviour of F, Q by means of the first equations in (4.2d, e) respectively. In practice, the first station in $\tilde{X}$ is taken at $1 + \Delta$ with Δ positive but tiny, and a_0 is evaluated by equating the known F at that station with $a_0 \Delta^{1/2}$; likewise for α_0, from Q and $\alpha_0 \Delta^{-1/2}$; then ℓ_1 gives ℓ' and hence a new-time ℓ value. Next, new P values at all $\tilde{X}$ stations are obtained directly from a discretized version of (4.1c), given F, Q. Following that, the program marches inwards in $\tilde{X}$, starting with the farfield condition imposed as in (2.5), to yield new Q, F respectively from (4.1a,b) in discretized form for all $\tilde{X}$, ending at $\tilde{X} = 1 + \Delta$. This inward march is based on passing information along the characteristics $d\tilde{X}/dT = -\ell' \tilde{X}/\ell$, i.e. $X =$ constant, and on evaluating the Cauchy-Hilbert integral in (4.1a) at each $\tilde{X}$ station using the latest P values. The program is then ready for the next time step. Double-marching in $\tilde{X}$ is also applied to achieve higher spatial accuracy. The transformation to χ enables high resolution of (4.2a–e) locally along with a large end value $\tilde{X}_\infty$ for $\tilde{X}$ at which to impose (2.5). Typically, we took χ_∞ greater than 0.95 ($\pi/2$), and we worked in terms of a transformed $\partial P/\partial X$ instead of the pressure.

The results are shown in Figure 3(a–e). These include cases which accommodate a fixed bump on the wall, represented by the scaled shape $S(X)$, whose influence can be followed by subtracting $S(\ell \tilde{X})$ from $F(\tilde{X}, T)$ in (4.1c) alone. The solutions in Figure 3(a–e) have the specific bump shape $S = H \exp\{-2(X - 3)^2\}$ with constant height factor H and start at $T = 1$ with the ideal solution imposed. Plots of the scaled interface shape F against $\tilde{X}$ at various T and the corresponding evolution of the contact half-length ℓ and the eigenfunction coefficient $\hat{v}$ are presented in Figure 3(a,b) for H zero (no bump). At first sight, and because of the use of the $\tilde{X}$ coordinate, it may appear that the interface is moving away from the horizontal axis with increasing time but the opposite is true in the $X - T$ plane, i.e. the interface approaches the axis. The case in Figure 3(a,b) has the interesting feature that $\hat{v}$ reaches a small positive minimum followed by a steep rise, while nearby ℓ almost develops a kink in the sense that the slope of ℓ against T changes rapidly. The effects of nonzero H are then shown in Figure 3(c, d) for the same value of Γ. Increasing H to 1 smooths out the development seen in Figure 3(b), whereas reducing H to -1 instead forces $\hat{v}$ to reach down to zero at a finite scaled time, accompanied by a local drop in the ℓ solution, at which stage the solution fails. Figure 3(e) has a decreased value of Γ, but the influence of reducing H from zero to -1.5 and then to -6 produces trends which are similar to those above even if of a different scale. The interpretation of the effect of the

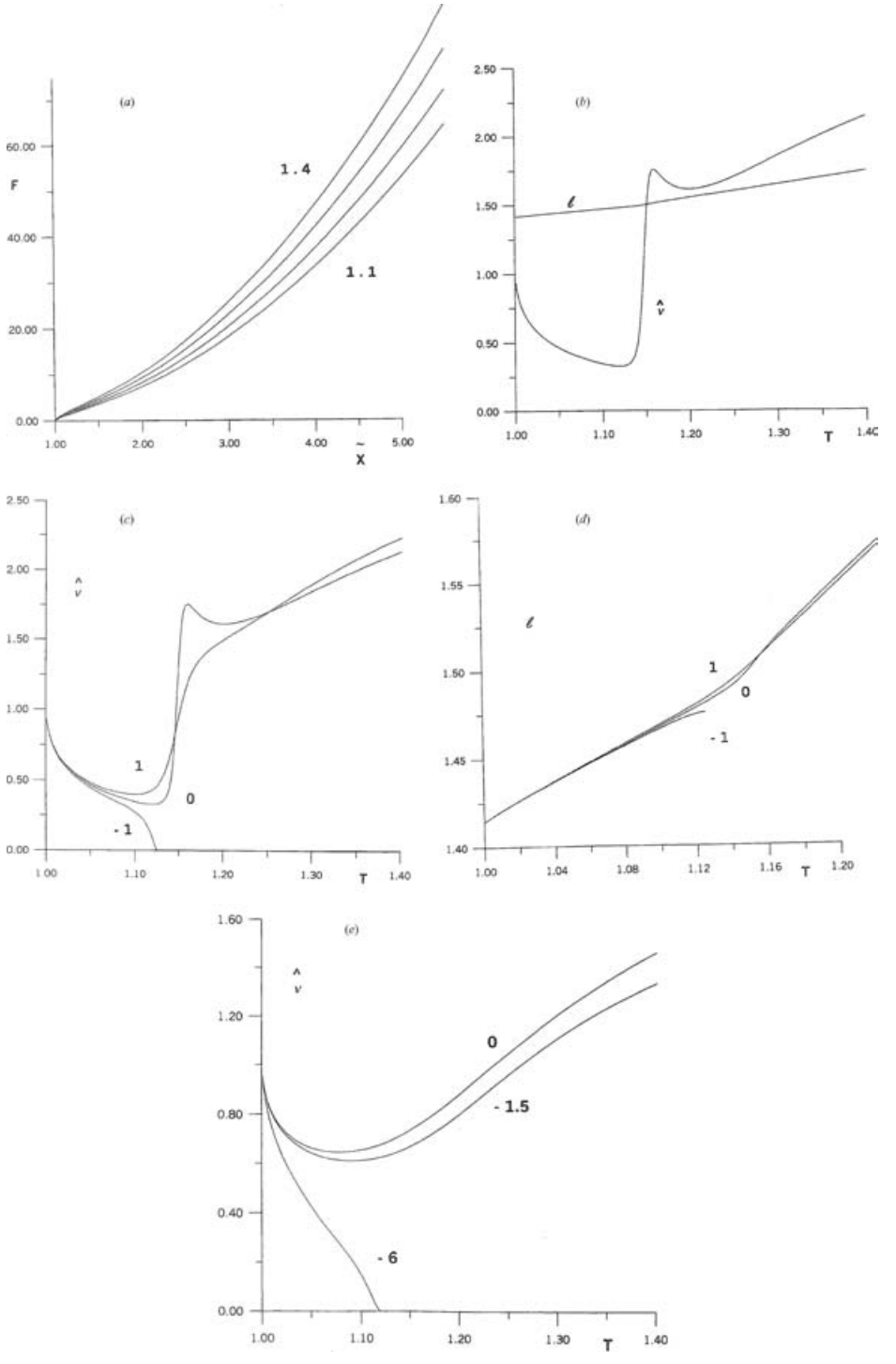

FIGURE 3. Computational solutions of (4.1a–c) with $(a-d)$ $\Gamma = 1.208$, (e) $\Gamma = 0.833$. Grid has $\tilde{X}_\infty > 160$. (a) F versus $\tilde{X}$ at times $T = 1.1,\ 1.2,\ 1.3,\ 1.4$, as shown. (b) ℓ, $\hat{v}$ versus T for the case of (a). (c)–(e) include bump shape $H\exp[-2(X-3)^2]$: (c), (d) ℓ, $\hat{v}$ for various H values; (e) $\hat{v}$ for $H = 0, -1.5, -6$ as indicated.

bump in each case is delicate because of the inherent nonlinearity and global integration but, in broad terms, increasing the height factor H appears equivalent to a reduction in Γ and hence reduces the air-motion effect. Decreasing H produces the opposite trend. This is similar to a blocking effect and is not unrelated to the determination of the constant ϕ_0 in (4.3). (Some bump effects on pre-impact interactions, as opposed to the present post-impact ones, are included implicitly in Smith *et al.*'s 2003 results, and only affect the touchdown position then.) Overall the results suggest that for a given configuration and initial condition there is an $O(1)$ cut-off value of Γ or, for given Γ, a cut-off value of $\max|S|$. At cut-off the coefficient $\hat{v}$ just touches zero, while below cut-off $\hat{v}$ remains positive throughout and above cut-off $\hat{v}$ reaches zero at a finite scaled time and the contact length stops increasing. *Below cut-off*, in fact, after significant air-water interaction the air effects eventually fade away to leave

$$\ell \sim (2T)^{1/2}, \quad \hat{v} \to 1 \quad \text{as} \quad T \to \infty, \tag{4.4a}$$

i.e. the air-negligible case, in which the asymptote of (4.1a–c) is

$$F \sim \tilde{X}(\tilde{X}^2-1)^{1/2}\ell^2, \quad Q \sim -\tilde{X}(\tilde{X}^2-1)^{-1/2}, \quad |P| \sim T^{-2} \tag{4.4b}$$

for large T. *Above cut-off,* by contrast, the air-water interaction appears to lead to a termination of the assumed flow structure within a finite time, $T = T_0^*$ say, with the local coefficient $\hat{v}$ tending to zero then.

The overall inference then is that sufficiently strong air motion in the gap or a sufficiently pronounced roughness (or roughnesses) can so alter both the air and water flow responses that the contact length ℓ is altered substantially from the pure water case and even a breakdown and change of flow structure seem to be forced to occur. Weak air motions or roughnesses on the other hand only provoke effects which die out. Analytical support for this inference, which we repeat is in the absence of surface tension, is considered below.

The *near-cut-off or marginal* situation admits of an analysis as follows. From the orders of magnitude in (4.1a–c) the solution responds on a short scale, close to the contact point, at times near some constant value T_0, such that

$$\ell = \ell_0 + \delta_1 L + \cdots, \quad \hat{v} = \epsilon N + \cdots, \tag{4.5a}$$

$$T - T_0 = \delta_1 \tilde{t}, \quad \tilde{X} - 1 = \delta_1 \tilde{x}, \tag{4.5b}$$

where ϵ, δ_1 are assumed small with $\delta_1 \ll \epsilon^6$, and

$$F = \epsilon \delta_1^{1/2} \tilde{f} + \cdots, \quad q = \epsilon \delta_1^{-1/2} \tilde{q} + \cdots. \tag{4.5c}$$

The corresponding pressure P induced on the short scale is of order ϵ^{-2} due to (4.1c) and this provokes, via the integral in (4.1a), a contribution that is small compared with the $\hat{v}$ contribution provided $\delta_1 \ll \epsilon^6$. The longer-scale contribution from the integral is then substantial however (compare (4.3)) as it provides the final term $\propto \kappa_3$ in the first of the two equations obtained from (4.1a,b), namely

$$\tilde{q}_{\tilde{t}} - \kappa_1 L'(\tilde{t})\tilde{q}_{\tilde{x}} = -\kappa_2 N/\tilde{x}^{3/2} + \kappa_3/\tilde{x}^{1/2}, \tag{4.6a}$$

$$\tilde{f}_{\tilde{t}} - \kappa_1 L'(\tilde{t})\tilde{f}_{\tilde{x}} = \tilde{q}. \tag{4.6b}$$

The prime denotes $d/d\tilde{t}$, the constants κ_1-κ_3 can be supposed known with κ_1, κ_2 positive, and only the range $\tilde{x} > 0$ is of concern. The solution of (4.5a,b) then has the form

$$\tilde{q} = A_1\tilde{x}^{-1/2} + A_2\tilde{x}^{1/2}, \quad \tilde{f} = A_3\tilde{x}^{1/2} + A_4\tilde{x}^{3/2} \tag{4.7}$$

where A_{1-4} are unknown functions of $\tilde{t}$. Substitution into (4.5a,b) leads to a nonlinear equation for $L(\tilde{t})$ and a linear one for $N(\tilde{t})$:

$$\frac{1}{2}\kappa_1 L'(\tilde{t})\left\{\frac{3}{2}\kappa_1 A_4 L + A_2\tilde{t} + \kappa_5\right\} = -\left\{\frac{1}{2}\kappa_1 A_2 L + \kappa_3\tilde{t} + \kappa_4\right\}, \tag{4.8a}$$

$$\kappa_2 N = -\frac{1}{2}\kappa_1 L'(\tilde{t})\left\{\frac{1}{2}\kappa_1 A_2 L + \kappa_3\tilde{t} + \kappa_4\right\}. \tag{4.8b}$$

Here A_2, A_4 have to be constant for self-consistency, A_1, A_3 are given by the expressions inside the curly brackets on the right- and left-hand sides of (4.8a), respectively, and κ_4, κ_5 are constants of integration. Hence we obtain the expressions

$$\bar{L} = \pm\bar{t} \pm \{(1 - \bar{\lambda}_1)\bar{t}^2 + \bar{\lambda}_2\}^{1/2}, \tag{4.9a}$$

$$\bar{N} = (\bar{L} \pm \bar{\lambda}_1\bar{t})^2/(\bar{L} \pm \bar{t}) \tag{4.9b}$$

in normalized variables where $L = \bar{L}_0 + |\bar{b}_1|^{-1}\bar{L}$, $T = \bar{T}_0 + |\bar{b}_2|^{-1}\bar{t}$, the constants $\bar{L}_0, \bar{T}_0$ are fixed by

$$\begin{cases} \frac{3}{2}\kappa_1 A_4\bar{L}_0 + A_2\bar{T}_0 + \kappa_5 = 0, \\ \frac{1}{2}\kappa_1 A_2\bar{L}_0 + \kappa_3\bar{T}_0 + \kappa_4 = 0, \end{cases}$$

and $\bar{b}_1 \equiv 3\kappa_1^2 A_4/4$, $\bar{b}_2 \equiv \kappa_1 A_2/2$, $\bar{\lambda}_1 \equiv \bar{b}_1\kappa_3/\bar{b}_2^2$, while $\bar{\lambda}_2$ is a constant of integration. The constants $\bar{\lambda}_1, \bar{\lambda}_2$ in (4.9a,b) may therefore be positive or negative, although only the regime $\bar{\lambda}_1 \leqslant 1$ has real relevance here. Again, the first plus sign in (4.9a) corresponds to $\bar{b}_1\bar{b}_2 < 0$, the first minus to $\bar{b}_1\bar{b}_2 > 0$, but the opposite is true in (4.9b). The near-critical solutions (4.9a,b) are plotted in Figure 4(a,b). In Figure 4(a), $\bar{\lambda}_1$ is 0.1 or -0.3, with $\bar{\lambda}_2$ kept at unity, and the plus signs apply in (4.9a). This corresponds to the subcritical regime, giving $\bar{L}$ linear when $\bar{t}$ is large and negative or large and positive but with different slopes then, and likewise for $\bar{N}$, although the changes in slope in $\bar{N}$ are numerically quite larger. Figure 4(b), on the other hand, has $\bar{\lambda}_1 = 0.5$ but $\bar{\lambda}_2$ is -1, and the two cases shown are due to the signs on the square roots above. Figure 4(b) is in the supercritical regime, with the solution terminating at $\bar{t} = \bar{t}_0 = -\sqrt{2}$, where $\bar{L}$ tends to $-\bar{t}_0$, but encounters a square-root singularity and $\bar{N}$ tends to $\pm\infty$ as indicated. Depending on the parameters and signs involved the solutions can clearly, among other things, describe evolutions in which the slope of ℓ versus T changes significantly over a short time scale ($\bar{t}$) or in which $\hat{v}$ tends to zero from above at a finite $\bar{t}$. These evolutions in particular appear to reflect well the properties found numerically in Figure 3 for the full system (4.1a–c) near the cut-off values.

5 Further comments

The theory has focused on two distinct and specific aspects of air-water interaction: surface tension acting just before impact and interaction phenomena just after impact.

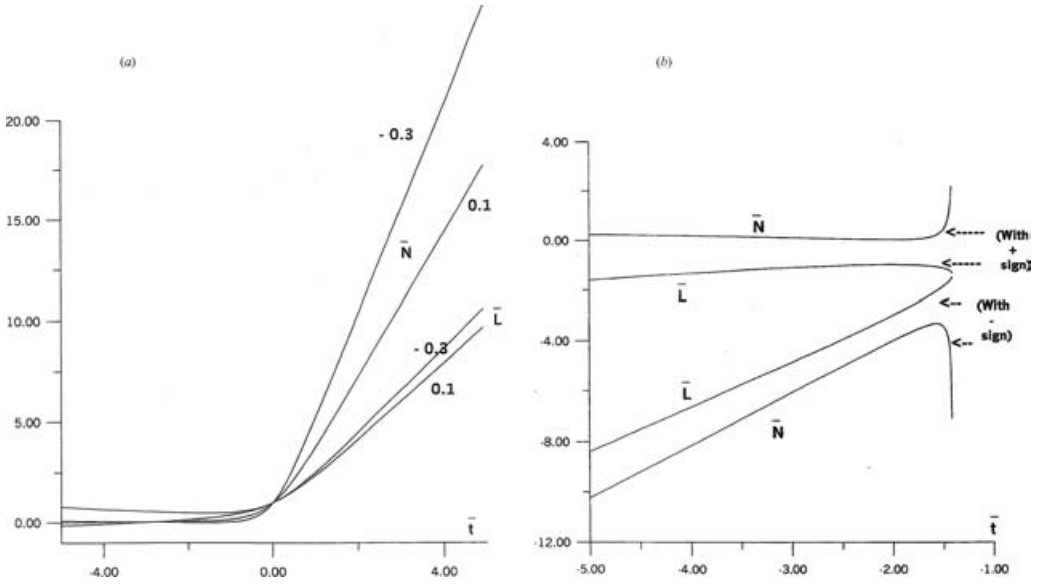

FIGURE 4. Near-critical solutions (4.9a,b) for $\bar{L}, \bar{N}$ against $\bar{t}$: (a) $\bar{\lambda}_2 = 1$, $\bar{\lambda}_1 = 0.1$ and -0.3 as shown, with plus signs in (4.9a); (b) $\bar{\lambda}_2 = -1$, $\bar{\lambda}_1 = 0.5$, where the two cases shown are for the different signs in (4.9a,b).

Concerning surface tension, the main effect is a significant delay of touchdown (§ 3) compared with the case of zero surface tension, even though it should be remarked again that the parameter involved is small in the real situations of present concern. The length and time scales may be tiny then (§ 3), readily admitting several other influences such as air inertia or relative non-thinness of the air gap. We reiterate that the relation between the original impact for zero surface tension and the inhibited impact otherwise is described at the end of § 3 and fits within the present model. Concerning post-impact phenomena, the general slowing down found (in § 4) due to the presence of air dynamics is also observed in recent direct numerical simulations incorporating air motion (e.g. by Purvis & Smith, 2004). Indeed, the present findings imply that the spreading of the water droplet can in a sense become stalled, and involve a local change of flow structure (the singular time T_0^* quoted in § 4 being given by T_0 at first). Taking this a little further, one has the intriguing possibility that the singularity factor or eigen-function coefficient $\hat{v}$ in (4.1a), which helps dictate the strength of the square-root interfacial shape near contact, remains zero after the structural change above. In such an event a similarity solution of the governing equations in (4.1a–c) would suggest that the spread position, i.e. half-length of contact, $\ell(T)$ responds as

$$\ell \sim T^{1/2} \text{ as } T \to \infty, \tag{5.1}$$

because of the farfield condition along with the absence of $\hat{v}$. Again, the slowing down, in comparison with ℓ in (4.4a), is evident. It would be interesting to know the additional influence of surface tension in the post-impact setting.

Many other influences are also of concern, needless to say. These include incidence in the droplet approach, water layer depth, background air and water motion, other viscous and

thermal effects, impact-impact interaction, compressibility, gravity and ice-wall roughness. Models and governing equations for some of them have been studied already. Also the inviscid, rather than lubricating, dynamics of the air in air-water interactions has interest even if the Reynolds number then has to be above the order of 10 million (from $v_2\rho_1^2/(v_1\rho_2^2)$). There is indeed a parallel theory for such higher momentum drops, which have $\mathrm{Re}_1 \gg v_2\rho_1^2/(v_1\rho_2^2)$ and so have (2.4) replaced by

$$F_T + (UF)_X = 0, \text{ where } U_T + UU_X = -P_X, \tag{5.2}$$

as in Wilson (1991) and Smith *et al.* (2003). For completeness the resulting analogues of § 3, 4 are described briefly in the appendix. A further investigation is under way in collaboration with Professor J.-M. Vanden-Broeck. Pre-existing air streams and layers are likewise amenable to analysis.

Acknowledgements

Interest and helpful discussions with Roger Gent and Richard Moser of QinetiQ, David Allwright of the Smith Institute, and David Hammond and Manolo Quero of Cranfield, are gratefully acknowledged, as is the support of EPSRC and QinetiQ through the Faraday Partnership for Industrial Mathematics, managed by the Smith Institute. John Lister kindly noted three references. The referees' and editors' helpful comments are also gratefully acknowledged.

Appendix A Higher momentum droplets

Here (5.2) is coupled with (2.6) in the pre-impact stage.

First, for zero σ, fine grid computations performed suggest secondary instability. Analytically, short-scale disturbances $\propto \exp(ikx+qt)$ about a basic solution $[F, P, U]$ say yield for large k the dispersion relation

$$q^2 = |k|(U^2F^{-1} - k^2\sigma) \tag{A 1}$$

from (2.6), (5.2). This confirms the presence of secondary instability at zero σ where $q \propto |k|^{1/2}$ is real for all k. Essentially the same result was obtained separately and by different means by Oliver (2002). Second, for nonzero σ however only secondary waves are implied at larger $|k|$ values since q becomes pure imaginary. Numerical results for nonzero σ are presented in Figure 5(a,b), for a horizontally symmetric configuration and a nonsymmetric one, respectively; the latter (which shows both F and P) is created by adding an air stream from left to right which is imposed by means of the farfield conditions. The results seem equivocal at first since the former tends to point to wave-like behaviour and the latter to touchdown or near-touchdown at a finite time $T = T_h$ say.

Third, for possible touchdown the orders of magnitude in (2.6), (5.2) indicate a form, local to the touchdown position X_h,

$$[F, P, U] \sim \left[(T_h - T)^{\hat{n}}\hat{F}, \quad (T_h - T)^{\hat{n}-4/3}\hat{P}, \quad (T_h - T)^{\hat{n}/2-2/3}\hat{U}\right] \tag{A 2}$$

with the length scaling as $X - X_h = (T_h - T)^{2/3}\hat{\xi}$, where $\hat{\xi} \sim 1$ and $0 < \hat{n} < \frac{2}{3}$. Hence the

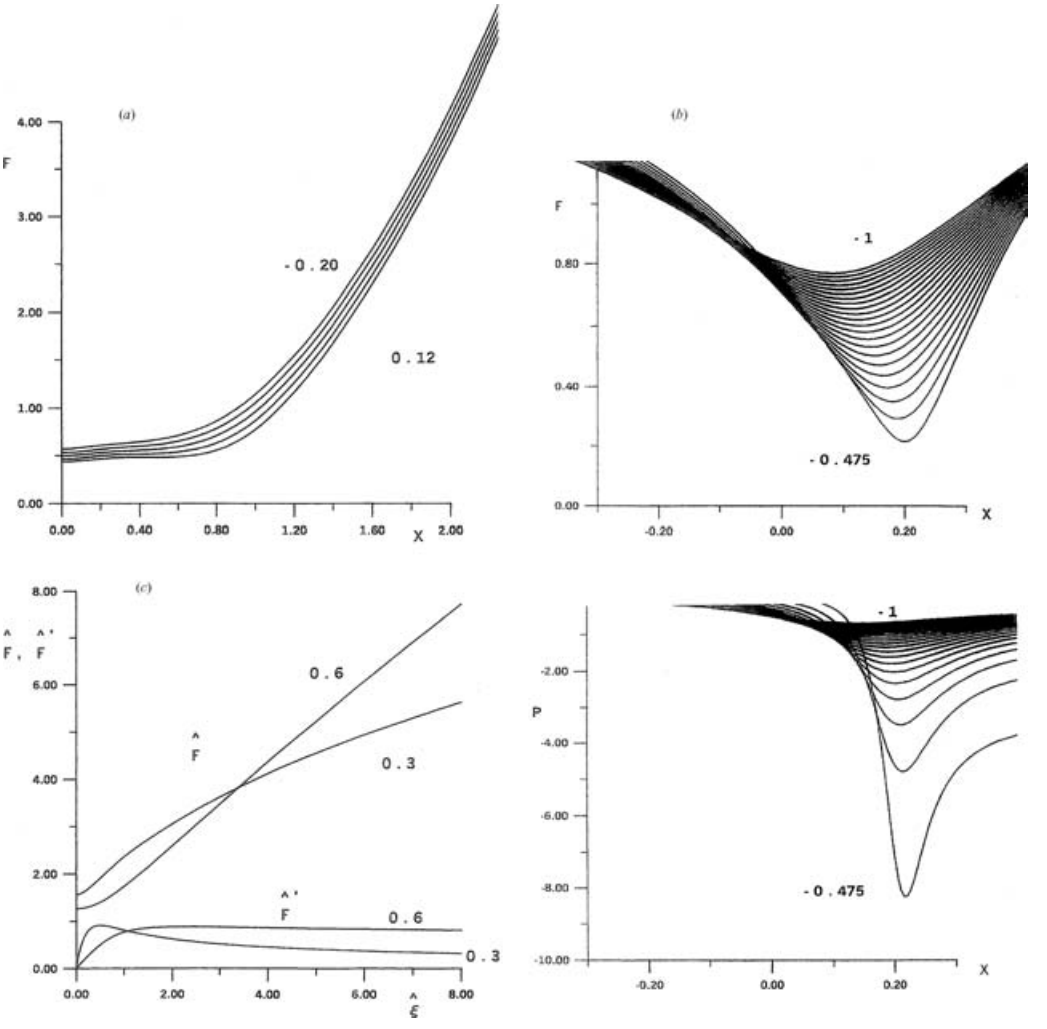

FIGURE 5. For the higher momentum droplets studied in the appendix: (a) solutions of (2.6), (5.2) at times T shown, with $\sigma = 0.002$ and symmetry about $X = 0$; (b) as (a) but $\sigma = 0.02$ and nonsymmetry, showing F (upper) and P (lower); (c) solution of (A3) for $\hat{n} = 0.3, 0.6$, with σ zero.

nonlinear governing equation

$$\tfrac{2}{3}\hat{\xi}^2\hat{F}'' + \left(\tfrac{5}{3} - 2\hat{n}\right)\hat{\xi}\hat{F}' + \tfrac{3}{2}\hat{n}(\hat{n}-1)\hat{F} = \frac{3}{2\pi}\int_{-\infty}^{\infty}\left(\frac{c_1^2\hat{F}'}{\hat{F}^3} + \sigma\hat{F}'''\right)\frac{d\xi}{\hat{\xi}-\xi} \tag{A 3}$$

applies, subject to the matching condition $\hat{F} \propto |\hat{\xi}|^{3\hat{n}/2}$ as $|\hat{\xi}| \to \infty$, and $\hat{F} > 0$. Here the prime denotes differentiation with respect to $\hat{\xi}$ and c_1 is a constant, with $\hat{U}$ given by c_1/F and $\hat{P}$ by $-c_1^2/(2\hat{F}^2)$ to within an additive constant. The solution for small $\hat{n}$ can be derived analytically,

$$\hat{F} = A_0 + \hat{n}\hat{F}_1 + 0(\hat{n}^2), \quad \hat{F}_1' \equiv A_1\hat{\xi}\int_0^{\infty}\frac{e^{-\kappa s}s^{5/2}ds}{(1+s^2\hat{\xi}^2)}, \tag{A 4}$$

where A_0, A_1 are positive 0(1) constants and $\kappa \equiv 9c_1^2/(4A_0^3)$. This holds only for σ zero, however. We could find no solution otherwise. Similarly, over the range of $\hat{n}$ values from 0 to 2/3 numerical solutions of (A3), derived by using (A4) as a first guess, could be obtained only for σ zero; these are shown in Figure 5(c) and are in line with (A4) as $\hat{n}$ decreases. We should remark that the pressure becomes large and negative in this touchdown, as opposed to the pressure in Smith *et al.*'s (2003) case which is generally large and positive and which therefore seems closer to the experimental findings in Lesser & Field (1983). Again, the existence of a touchdown solution as in (A2)–(A4) and fig.5(c) over a range of values of $\hat{n}$ rather than for just a single $\hat{n}$ value ties in with the presence of short-length instability in (A1) when σ is zero. No touchdown solutions could be found for σ nonzero, whatever the $\hat{n}$ value.

Finally, the corresponding post-impact theory analogous with that in §4 is likewise based on (5.2) replacing (2.4). Thus (4.1c) is then replaced by $\ell Q + \partial(UF)/\partial\tilde{X} = 0$ where $\ell\partial U/\partial T + (U - \ell'\tilde{X})\partial U/\partial\tilde{X} = -\partial P/\partial\tilde{X}$, while (4.1a,b) remain unaltered. Moreover, the cut-off at finite time and finite parameter values in the form (4.5a)–(4.9b) remains possible since the cut-off is not affected by the precise nature of (4.1c) or its replacement just above in the present case but by the longer-scale contribution κ_3 in (4.6a).

References

[1] Beretta, E. (1997) Self-similar source solutions of a fourth order degenerate parabolic equation. *Nonlinear Anal., Theory, Meth. & Applic.* **7**, 741–760.

[2] Braun, R. J. & Fitt, A. D. (2003) Modelling drainage of the precorneal tear film after a blink. *Math. Med. & Biol.* **20**, 1–28.

[3] Greenspan, H. P. (1978) On the motion of a small viscous droplet that wets a surface. *J. Fluid Mech.* **84**, 125–143.

[4] Gueyffier, D., Li, J., Nadim, A., Scardovelli, R. & Zaleski, S. (1999) Volume of fluid interface tracking with smoothed surface stress methods for three-dimensional flows. *J. Comp. Phys.* **152**, 423–456.

[5] Howison, S. D., Ockendon, J. R. & Wilson, S. K. (1991) Incompressible water-entry problems at small deadrise angles. *J. Fluid Mech.* **222**, 215–230.

[6] Howison, S. D., Ockendon, J. R. & Oliver, J. M. (2002) Deep- and shallow-water slamming at small and zero deadrise angles. *J. Eng. Maths.* **42**, 373–388.

[7] Jensen, O. E. (2000) Draining collars and lenses in liquid-lined vertical tubes. *J. Colloid. Interface Sci.* **221**, 38–49.

[8] Josserand, C. & Zaleski, S. (2003) Droplet splashing on a thin liquid film. *Physics of Fluids*, **15**, 1650–1657.

[9] Kalliadasis, S. & Chang, H. C. (1994) Drop formation during coating of vertical fibres. *J. Fluid Mech.* **261**, 135–168.

[10] Kang, Y. & Vanden-Broeck, J.-M. (2000). Gravity-capillary waves in the presence of constant vorticity. *Euro. J. Mech. B*, **19**, 253–268.

[11] King, A. C. & Tuck, E. O. (1993) Thin fluid layers supported by surface traction. *J. Fluid Mech.* **251**, 709–718.

[12] King, A. C., Tuck, E. O. & Vanden-Broeck, J.-M. (1993) Air-blown waves on thin viscous sheets. *Phys. Fluids A*, **5**, 973–978.

[13] Korobkin, A. A. (1997) Asymptotic theory of liquid-solid impact. *Phil. Trans. R. Soc. Lond. A* **355**, 507–522.

[14] Korobkin, A. A. (1999) Shallow water impact problems. *J. Eng. Maths.* **35**, 233–250.

[15] Kriegsmann, J. J., Miksis, M. J. & Vanden-Broeck, J.-M. (1998) Pressure driven disturbances on a thin viscous film. *Phys. Fluids*, **10**, 1249–1255.
[16] Lesser, M. B. & Field, J. E. (1983) The impact of compressible liquids. *Ann. Rev. Fluid Mech.* **15**, 97–122.
[17] Liow, J. L. (2001) Splash formation by spherical drops. *J. Fluid Mech.* **427**, 73–105.
[18] McKinley, I. S. & Wilson, S. K. (2001) The linear stability of a ridge of fluid subject to a jet of air. *Phys. Fluids*, **13**, 872–883.
[19] Miksis, M. J. & Vanden-Broeck, J.-M. (1999) Self-similar dynamics of a viscous wedge of fluid. *Phys. Fluids*, **11**, 3227–3231.
[20] Oliver, J. M. (2002) Water entry and related problems. PhD thesis, University of Oxford.
[21] Purvis, R. & Smith, F. T. (2004) Large droplet impact on water layers. AIAA paper AIAA-2004-0414, 42nd Aerosp. Sci. Conf. & Exhib., Reno, NV.
[22] Purvis, R. & Smith, F. T. (2005) Droplet impact on water layers: post-impact analysis and computations. *Phil. Trans. Roy. Soc. A* (in press).
[23] Smith, F. T., Li, L. & Wu, G.-X. (2003) Air cushioning with a lubrication/inviscid balance. *J. Fluid Mech.* **482**, 291–318.
[24] Tuck, E. O. & Schwartz, L. W. (1990) A numerical and asymptotic study of some 3rd-order ordinary differential equations relevant to draining and coating flows. *SIAM Rev.* **32**, 453–469.
[25] Vanden-Broeck, J.-M. & Miloh, T. (1996) The influence of a layer of mud on the train of waves generated by a moving pressure distribution. *J. Eng. Maths.* **30**, 387–400.
[26] Wilson, S. K. (1991) A mathematical model for the initial stages of fluid impact in the presence of a cushioning fluid layer. *J. Eng. Maths.* **25**, 265–285.